optica

Plasmonic and diffractive nanostructures for light trapping—an experimental comparison

Christian S. Schuster,[1,*] Seweryn Morawiec,[2] Manuel J. Mendes,[2] Maddalena Patrini,[3] Emiliano R. Martins,[4] Liam Lewis,[5] Isodiana Crupi,[2] and Thomas F. Krauss[1]

[1]Department of Physics, University of York, York, YO10 5DD, UK

[2]MATIS CNR-IMM and Department of Physics and Astronomy, University of Catania, Via S. Sofia 64, 95123 Catania, Italy

[3]Department of Physics, University of Pavia, Via Bassi 6, 27100 Pavia, Italy

[4]Departamento de Física, Universidade Federal de São Carlos, 13565-905 São Carlos, São Paulo, Brazil

[5]Photonics Device Dynamics Group, Tyndall National Institute, Lee Maltings, Cork, Ireland

*Corresponding author: christian.schuster@york.ac.uk

Metal nanoparticles and diffractive nanostructures are widely studied for enhancing light trapping efficiency in thin-film solar cells. Both have achieved high performance enhancements, but there are very few direct comparisons between the two. Also, it is difficult to accurately determine the parasitic absorption of metal nanoparticles. Here, we assess the light trapping efficiencies of both approaches in an identical absorber configuration. We use a 240 nm thick amorphous silicon slab as the absorber layer and either a quasi-random supercell diffractive nanostructure or a layer of self-assembled metal nanoparticles for light trapping. Both the plasmonic and diffractive structures strongly enhance the absorption in the red/near-infrared regime. At longer wavelengths, however, parasitic absorption becomes evident in the metal nanoparticles, which reduces the overall performance of the plasmonic approach. We have formulated a simple analytical model to assess the parasitic absorption and effective reflectivity of a plasmonic reflector and to demonstrate good agreement with the experimental data.   © 2015 Optical Society of America

1. INTRODUCTION

Thin films are a promising approach for not only further reducing the cost of solar cells, but also for increasing their efficiency via the open-circuit voltage [1]. Thin-film technologies strongly benefit from light-trapping approaches because the required absorption length may exceed the cell thickness, especially at longer wavelengths.

Metal nanoparticle scatterers and diffractive nanostructures have been widely studied for light trapping, and both concepts have been shown to enhance the absorption efficiency [2–5]. A direct comparison on identical absorber layers has not yet been carried out, however. The difficulty of such a comparison is to keep the absorber material properties constant, to use an

identical antireflection coating layer on the illumination side, and to properly account for any parasitic effects such as absorption in the metal nanoparticles or in any contact layer. The experiment reported here addresses these challenges and thereby affords a fair comparison between plasmonic and diffractive light trapping. In order to minimize the number of parameters, we conducted the comparison on a simple slab of amorphous silicon (a-Si) on a glass substrate, i.e., without the usual rear mirror implemented in plasmonic backreflectors [6–8]. The thickness of the a-Si layer is 240 nm and is close to the value used in thin-film solar cells [8]. For the diffractive approach, we used the quasi-random supercell design [9,10], which we demonstrated previously as one of the most

effective diffractive nanostructures [11]; for the plasmonic approach, we used a layer of self-assembled silver nanoparticles, which has shown some of the strongest light trapping performance among metallic nanostructures [6,12]. The two types of structures are shown in Fig. 1. The absorber material and its processing were identical in both cases, whereas the absorption measurements were performed in two laboratories in to cross-check the experimental results.

2. DESIGN AND FABRICATION

The quasi-random supercell design can provide outstanding light trapping [10], while relying on only a binary grating approach that could be mass-produced using the nanoimprint technology [13]. The high performance of the design is explained by a Fourier analysis [see bottom sketch in Fig. 1(a)]: the structure channels more energy into the higher diffraction orders that can couple into the quasi-guided modes of the thin film, thereby increasing the path length [14].

The plasmonic design consists of self-assembled silver nanoparticles. We chose silver (Ag) because it has a low imaginary permittivity and a high scattering efficiency in the visible and near-infrared spectra [15]. Here the nanoparticles are in direct contact with the high-index a-Si layer, in order to maximize light coupling into the thin absorber layer [16]. In addition, the nanoparticles are situated on the rear side of the absorber layer as this configuration is more advantageous for light trapping than placing them at the front [17]. For the fabrication, we used the solid-state dewetting method [18], whereby a thin metal film spontaneously forms nanoparticles when annealed at temperatures of typically 300°C–500°C. This method meets four key requirements of the photovoltaic industry: simplicity, low cost, reproducibility, and scalability. Figure 1(b) shows the plasmonic nanostructure investigated in the experiment.

More detailed information about the fabrication of the structures, the material properties, measurements, and characterization methods can be found in Supplement 1.
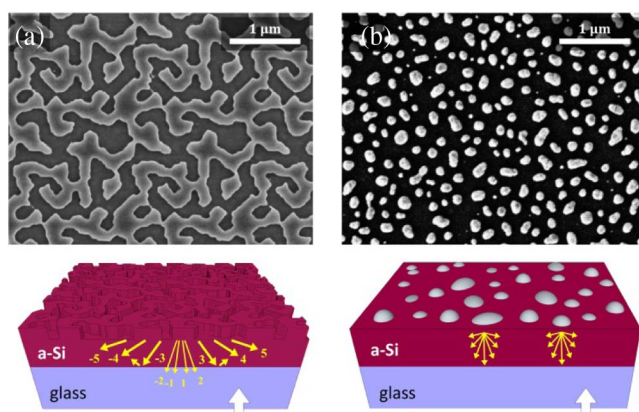
Fig. 1. (a) A diffractive 2D quasi-periodic nanostructure, optimized to channel more energy into the higher diffraction orders. (b) A plasmonic nanostructure designed to scatter light efficiently into the silicon layer. Both approaches have been realized on the back of a 240 nm a-Si absorber slab. The white arrows in the bottom sketches indicate the illumination direction.

3. RESULTS

All measurements are taken in superstrate configuration, where light enters through the glass–semiconductor interface. This arrangement affords a fair assessment of the scattering properties because it excludes antireflection properties. Figure 2 shows the measured total absorption of both structures with reference to an identical unstructured slab.

In the visible range of 550–700 nm, the quasi-random supercell outperforms the plasmonic nanoparticles, whereas the opposite is true in the near-infrared (700–1000 nm) where the plasmonic structure clearly causes higher light absorption. The key question is whether the additional absorption is due to stronger scattering of the plasmonic nanoparticles, or whether it is due to undesired parasitic absorption. Simple Mie theory suggests that for the particle sizes involved $(170 \pm 90 \text{ nm})$, parasitic absorption is minimal in the long-wavelength regime [7,19], but also that the scattering properties are very similar for thicker nanoparticles, as shown previously [12]. However, previous studies suggest that a high total absorption together with weak wavelength dependence, as observed here between 800 and 1000 nm, may be caused by parasitic contributions [20,21].

4. DISCUSSION

We suggest that the apparent discrepancy between Mie theory and the experimental observations [22] is mainly due to the multipass nature of light trapping; although the parasitic absorption for each reflection of the nanoparticles is indeed low, the near-infrared light being only weakly absorbed in the silicon layer makes many round trips and therefore samples the parasitic absorption many times, which accumulates to a sizeable absorption overall [23–25].

Therefore, we quantify the parasitic absorption by considering the attenuation of a propagating light ray in a lossy waveguide. Our simple model is a generalization of the model proposed by Gee [26] and is shown schematically in Fig. 3. It is based on the following three intuitive assumptions:

1. We assume incoherent scattering from the metal nanoparticles because the particles are broadly distributed and the light is randomized at every reflection. As a result, the (coherent) Fabry–Perot interference fringes around 600–700 nm are averaged out. Since averaging these fringes does not affect the
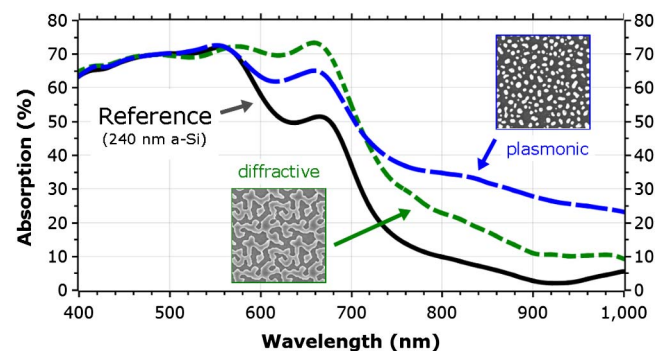
Fig. 2. Measured total absorption of the unstructured a-Si slab (black solid line), with an added diffractive structure (green short-dashed line) and with an added plasmonic structure (blue long-dashed line).
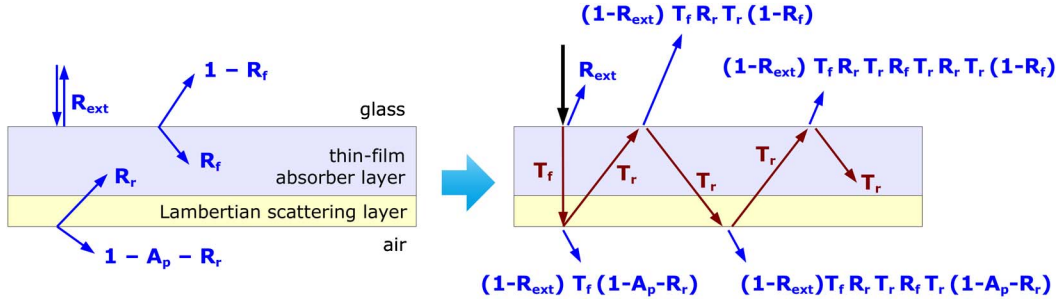
Fig. 3. When randomization of light at the scattering layer allows neglecting coherent effects, the propagation of an averaged light ray in a lossy waveguide is described by the external reflection R_{ext}, the internal effective reflectances R_f and R_r, the parasitic metal absorption A_p, and the attenuated transmission T_r with respect to the single-pass traversal T_f. We assumed the incident medium to be glass as all measurements were normalized to a reference glass cover slide.

integrated short-circuit current, noncoherence is an acceptable simplification.

2. We assume that the metal nanoparticles scatter Lambertionally. Lambertian scattering takes into account light that is coupled into the waveguide—in contrast to haze (the nonspecular part of reflection), which does not take waveguide coupling into account. We justify this assumption by the observation that the angular distribution of the scattered light was shown to be similar to the Lambertian case, when Ag nanoparticles were directly situated on the substrate [24].

3. Finally, we assume that scattering and parasitic absorption cannot be separated; once the light interacts with the nanoparticle resulting in scattering, it will be absorbed at the same time. This relationship is intrinsic to Mie theory and was highlighted recently by Sun and Khurgin [27]. As a result, minimizing parasitic losses is of critical importance for solar cell operation because the desired scattering properties are directly related to any loss channels.

The model starts with the single-pass transmission T_f through the silicon via the front glass interface. The light is then reflected and randomized by the nanoparticles and transmits again through the silicon. T_r refers to the averaged transmission of the randomized backscattered light rays. For absorbing media, T_r is always smaller than T_f because most lightpaths are longer compared with the first direct traversal:

$$T_r(\alpha) = \frac{1}{\pi} \int_0^{2\pi} d\varphi \int_0^{\pi/2} e^{-\alpha d \, \sec\theta} \cos\theta \sin\theta \, d\theta$$

$$= \int_0^{\pi/2} e^{-\alpha d \, \sec\theta} \sin 2\theta \, d\theta, \qquad (1)$$

where α and d are the absorption coefficient and slab thickness, respectively. The normalization factor $1/\pi$ as in Eq. (2) is required by energy conservation. In a transparent medium, photon–atom interactions only reduce the speed of light via photon absorption and re-emission processes [28], whereas in an absorptive medium, these interactions will also attenuate the intensity: the radiance of a Lambertian scatterer then loses its isotropic characteristic in the presence of absorption, which is reflected by the exponential term in Eq. (1). Our definition of T_r stands in contrast to a recently proposed model [29]

where Lambertionality was treated as independent of the constant α. The effective rear and front reflectances, R_r and R_f, respectively, are determined by the amount of light that leaves the absorber into the adjacent layers. Here R_r is used as a fitting parameter, whereas R_f can be calculated as the angle-averaged Fresnel reflection between a-Si and glass, assuming rotational symmetry:

$$R_f(\lambda) = \frac{1}{\pi} \int R_f(\lambda, \theta, \varphi) \, \boldsymbol{n} \cdot d\boldsymbol{\Omega}$$

$$= \int_0^{\pi/2} R_f(\lambda, \theta) \sin 2\theta \, d\theta. \qquad (2)$$

The more light is backscattered from the surface normal $\boldsymbol{n}$ into the differential solid angle $d\boldsymbol{\Omega}$ of a hemisphere, the higher the effective front reflection R_f. The factor $\sin 2\theta$ is derived in the same way as in Eq. (1). For a material with a small escape cone and a high refractive index n, Eq. (2) can be approximated by $1 - (n_{cladding}/n)^2$. The total absorption A_{tot} can now be calculated as

$$A_{tot} = Z\left[1 - T_f\left(1 - A_P - R_r\left(1 - T_r + R_f\left(1 - \frac{T_r}{T_f}\right)T_r\right)\right)\right].$$
$$(3)$$

The recirculation factor $Z = (1 - R_{ext})/(1 - R_r T_r R_f T_r)$ takes into account the attenuation of the average light ray due to the multiple upward and downward reflections at the cladding layers. For $T_f = 0$, all nonreflected light is absorbed, whereas for a transparent slab ($T_f = T_r = 1$), the total absorption is determined by A_p. Notice that the specular transmission is reproduced for $T_r = T_f$, where the single-pass absorption ($1 - T_f$) is enhanced by the product of R_r and T_f. The multipass nature of our model is highlighted by the absorption enhancement due to the randomization of the optical paths:

$$\frac{A_{tot}}{1 - T_f} = Z\left[1 + \frac{T_f}{1 - T_f}A_p + \eta \cdot R_r T_f + (\eta - 1) \cdot R_r R_f T_r\right].$$
$$(4)$$

Since T_r is always smaller than or equal to the transmittance T_f of a nonrandomized single-pass traversal, the factor

$\eta = (1 - T_r)/(1 - T_f)$ describes the enhancement due to randomization alone and is at best equal to 2 for weakly absorbed light [23]. Equation (4) naturally reproduces the Yablonovitch limit [30] for a Lambertian backscatterer to first-order approximation:

$$\frac{A_{\max}}{1 - T_f} \approx n^2 \left[1 + 0 + 2 \cdot 1 + 1 \cdot \left(1 - \frac{1}{n^2} \right) \right] = 4n^2 - 1.$$

$$(5)$$

Here, the theoretical maximum absorption enhancement is reduced by the first direct traversal as the $4n^2$ limit corresponds to a Lambertian front-scatterer with T_r replacing T_f in Eq. (3).

All parameters in Eq. (3) are known, except R_r (the effective backreflection from the nanoparticle layer) and A_p (the parasitic absorption). Following Morawiec et al. [12], we assume a constant value of the backreflection coefficient R_r, which is close to the experimental observation of Tan et al. [31] for the relevant wavelength range (600–1000 nm). Based on assumption 3 above, we therefore also assume a constant value for the absorption coefficient A_p.

For the analysis, we use the residual of the least-square method to find the best fitting parameter for R_r and A_p for the full wavelength regime between 400 and 1000 nm. The fitting outcome is shown as a contour plot in Fig. 4(a), allowing us to determine the best parameter set $(R_r, A_p) =$

(34%, 20%) directly from the plot. Figure 4(b) then compares the best fit with the measured data curve.

Since we have two fitting parameters, one may argue that the result is not unique, and it is true that a range of (R_r, A_p) values can be used to achieve a good fit in Fig. 4(b). However, the goal of the analysis is to determine the overall parasitic loss represented by the red curve in Fig. 4(b). Therefore, we varied the (R_r, A_p) values in the range of 25% < R_r < 50% and 13% < A_p < 25%, respectively, while maintaining a good fit to the experimental curve, and noted little variation of the red absorption curve as a result. This can also be understood intuitively: if R_r increases, the lightpath will be longer and the light experiences parasitic absorption more often; hence R_r and A_p are somewhat interchangeable without affecting the final result. Therefore, we note that the determination of the overall parasitic loss is very stable against parameter variations.

We can now plot the useful absorption alone by separating the parasitic contribution, which is shown in Fig. 5. We also include the unstructured reference and an ideal Lambertian backreflector. We find that over the full wavelength range, the quasi-random supercell outperforms the plasmonic design because the plasmonic structure extensively suffers from high parasitics in the long-wavelength regime.

At this point, we wish to point out that if the variation between differently sized plasmonic nanoparticles leads to only an ca. 10% variation in the scattering performance [12] and in haze in reflection [31], then Fig. 4 highlights the robustness of
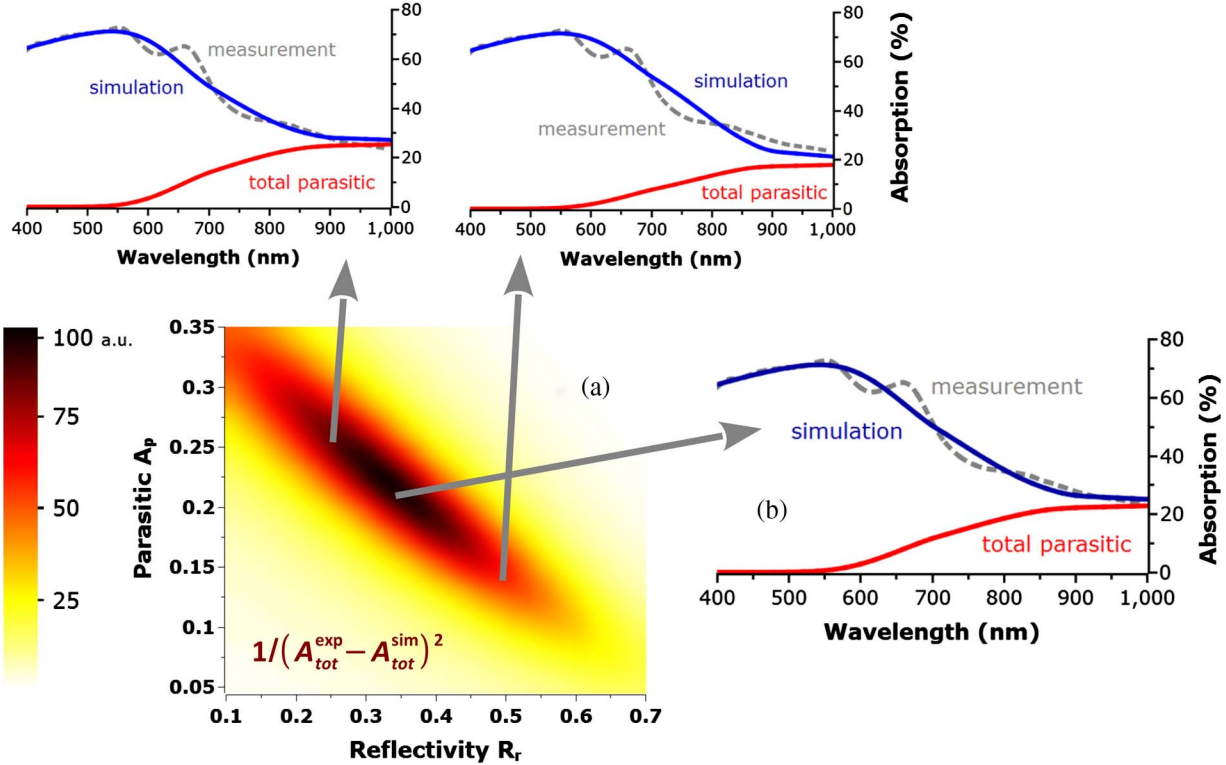
Fig. 4. Analysis of the modeled parasitic absorption caused by the metal nanoparticles. (a) Using the least-square method, the inverse of the residual between the simulated and measured total absorption A_{tot} is shown as a contour plot as a function of the effective backreflection R_r and the parasitic absorption A_p. (b) The measurement is then compared with the best fit with $R_r = 34\%$ and $A_p = 20\%$. Higher or lower values of R_r would overestimate either the measured absorption or the parasitics in the visible range, respectively, where most of the light does not reach the backscattering layer or only interacts once with the metal nanoparticles.
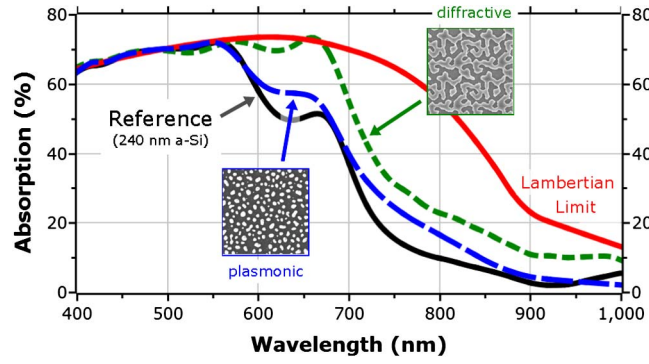
Fig. 5. Separating the parasitic contribution from the total absorption in Fig. 2, the graphs refer to the absorption in silicon only. Whereas the plasmonic structure (blue long-dashed line) can enhance the absorption of an unstructured a-Si slab (black solid line) by 7%, the diffractive structure (green short-dashed line) is able to do so by 25%. For comparison, the red solid line corresponds to the theoretical absorption of an ideal Lambertian backscatterer.

our analysis against any variations of this magnitude. However, to dispel remaining doubts on the generality of our conclusion, we demonstrate that no remarkable differences in the outcomes of our study are found when resonant and wavelength-dependent fitting parameters are included in the analysis (documented in Supplement 1).

Having determined the key parameters, we can proceed calculating the respective short-circuit currents and separate the useful absorption in the silicon from the parasitic absorption in the metal quantitatively. The implied short-circuit current J_{sc} of the plasmonic device can thus be calculated as

$$J_{SC} = \frac{e}{hc} \cdot \int_{400}^{1000} A_{\exp}(\lambda) \cdot \left[1 - \frac{A_{p,\text{tot}}(\lambda)}{A_{\text{tot}}(\lambda)} \right] \cdot \lambda \, \frac{dI}{d\lambda} \cdot d\lambda, \quad (6)$$

where we subtracted the total parasitics $A_{p,\text{tot}}$ from the measured absorption $A_{\exp}$. For simplicity, we assumed an internal quantum efficiency of unity over the AM1.5 global solar spectrum [32] $dI/d\lambda$. This simplification, however, must be dropped when the electric short-circuit current is assessed experimentally. For example, embedding our comparison into a solar cell would not only require more layers and (optical) interfaces, but the assessment would also necessarily involve additional effects, such as the electrical, chemical, and thermal properties of the device. The impact and interplay of these effects would screen the parameters we want to study and would make it more difficult to extract a clear conclusion in respect of the light-trapping mechanism itself. Here we do not try to address the question whether the best light-trapping strategy also maximizes the overall power conversion efficiency—this is a different research question beyond the scope of the present study.

Similarly, we also calculated the implied J_{sc} of the unstructured reference and of the diffractive structure, naturally without the A_p term. The result is shown in Table 1. We note a value of 14.6 mA/cm^2 for the plasmonic device and 17.1 mA/cm^2 for the diffractive device. We also show the light trapping efficiency (LTE), which we defined previously

Table 1. Comparison of the Integrated Silicon Absorption, the Calculated Short-Circuit Current J_{sc}, and the LTE [11] for the 400–1000 nm Wavelength Range

	Absorption	J_{sc} [a]	LTE
Unstructured reference	35.7%	13.5	0%
Plasmonic light trapping	38.3%	14.6	14.2%
Diffractive light trapping	44.8%	17.1	47.8%
Lambertian backscatterer	55.5%	21.3	100%

[a]in mA/cm^2.

as a figure of merit for light trapping [11] and which is unity for an ideal Lambertian scatterer.

5. CONCLUSIONS

We have carried out a direct comparison between two different light-trapping strategies for otherwise identical structures. Both structures were situated on the rear side of an absorber layer to afford a fair assessment of their scattering properties. In previous contributions, authors compared similar geometries [33] or plasmonic backreflectors with conventional textures [31,34,35], yet these studies were often biased toward a particular approach or experimental constraints had unavoidably penalized one of the concepts. Here we have assessed the light trapping efficiencies of plasmonic and diffractive structures experimentally and have formulated a simple analytical model in order to extract the parasitic absorption. In addition, our analysis still holds even for different types of parasitic absorption. Ingenito *et al.* [21] already proposed a similar method to differentiate between the absorptance in silicon and metal, yet their model does not facilitate the separate determination of the plasmonic nanoparticles' reflectivity and absorption in waveguide geometry.

The key difficulty in accurately modeling nonidentical and randomly distributed metal nanoparticles is caused by the random nature of the particles' shape, size, and volume as shown in Fig. 1(b). The lack of order, for example, leads to agglomerations and thus to enhanced interparticle interactions, which are known to reduce the plasmonic resonances [36,37]. Second, both the absorption and the scattering cross section

of a nanoparticle usually exceed the particle size, such that a computational cell is difficult to define. Plasmonic resonances are also quite sensitive to the area in contact with the substrate [24] as well as to defects in the nanoparticle's shell [15]. If a numerical computation were to include all of the above effects, the modeling would become complex or would run into convergence problems due to the required fine meshes.

Here we have found that a quasi-random supercell diffractive grating enhances the silicon absorption by 25% compared with an unstructured slab, whereas randomly distributed silver nanoparticles were able to do so by only 7%. Even though the high parasitics are responsible for the poor performance of the silver nanoparticles, they should be less detrimental in a real solar cell configuration because nanoparticles show a stronger scattering performance when coupled to a rear mirror [6,7,19].

The LTE related to the diffractive approach is so low because the supercell was originally designed for light in-coupling and would thus perform better on the front (LTE = 0.68). However, as the purpose of our study is a quantitative comparison, we opted to keep the parameters as identical as possible and thus accepted the reduction in the overall performance.

In conclusion, our work has shown that diffractive light trapping outperforms plasmonic light trapping due to cumulative parasitics arising from multipath interactions at longer wavelengths.

See Supplement 1 for supporting content.

REFERENCES

1. T. Tiedje, E. Yablonovitch, G. Cody, and B. Brooks, "Limiting efficiency of silicon solar cells," IEEE Trans. Electron Devices **31**, 711–716 (1984).
2. H. A. Atwater and A. Polman, "Plasmonics for improved photovoltaic devices," Nat. Mater. **9**, 205–213 (2010).
3. M. A. Green and S. Pillai, "Harnessing plasmonics for solar cells," Nat. Photonics **6**, 130–132 (2012).
4. F. Priolo, T. Gregorkiewicz, M. Galli, and T. F. Krauss, "Silicon nanostructures for photonics and photovoltaics," Nat. Nanotechnol. **9**, 19–32 (2014).
5. Z. Yu, A. Raman, and S. Fan, "Fundamental limit of nanophotonic light trapping in solar cells," Proc. Natl. Acad. Sci. USA **107**, 17491–17496 (2010).
6. S. Morawiec, M. J. Mendes, S. A. Filonovich, T. Mateus, S. Mirabella, H. Aguas, I. Ferreira, F. Simone, E. Fortunato, R. Martins, F. Priolo, and I. Crupi, "Broadband photocurrent enhancement in a-Si:H solar cells with plasmonic back reflectors," Opt. Express **22**, A1059–A1070 (2014).
7. M. J. Mendes, S. Morawiec, F. Simone, F. Priolo, and I. Crupi, "Colloidal plasmonic back reflectors for light trapping in solar cells," Nanoscale **6**, 4796–4805 (2014).
8. R. Santbergen, R. Liang, and M. Zeman, "a-Si:H solar cells with embedded silver nanoparticles," in *35th IEEE Photovoltaic Specialists Conference (PVSC)*, June 20–25, 2010, pp. 748–753.
9. E. R. Martins, J. Li, Y. Liu, and T. F. Krauss, "Engineering gratings for light trapping in photovoltaics: the supercell concept," Phys. Rev. B **86**, 041404 (2012).
10. E. R. Martins, J. Li, Y. Liu, V. Depauw, Z. Chen, J. Zhou, and T. F. Krauss, "Deterministic quasi-random nanostructures for photon control," Nat. Commun. **4**, 2665 (2013).
11. C. S. Schuster, A. Bozzola, L. C. Andreani, and T. F. Krauss, "How to assess light trapping structures versus a Lambertian scatterer for solar cells?" Opt. Express **22**, A542–A551 (2014).
12. S. Morawiec, M. J. Mendes, S. Mirabella, F. Simone, F. Priolo, and I. Crupi, "Self-assembled silver nanoparticles for plasmon-enhanced solar cell back reflectors: correlation between structural and optical properties," Nanotechnology **24**, 265601 (2013).
13. S. Y. Chou, P. R. Krauss, and P. J. Renstrom, "Imprint lithography with 25-nanometer resolution," Science **272**, 85–87 (1996).
14. H. W. Deckman, C. R. Wronski, H. Witzke, and E. Yablonovitch, "Optically enhanced amorphous silicon solar cells," Appl. Phys. Lett. **42**, 968–970 (1983).
15. P. R. West, S. Ishii, G. V. Naik, N. K. Emani, V. M. Shalaev, and A. Boltasseva, "Searching for better plasmonic materials," Laser Photon. Rev. **4**, 795–808 (2010).
16. A. M. Pennanen and J. J. Toppari, "Direct optical measurement of light coupling into planar waveguide by plasmonic nanoparticles," Opt. Express **21**, A23–A35 (2013).
17. Z. Ouyang, S. Pillai, F. Beck, O. Kunz, S. Varlamov, K. R. Catchpole, P. Campbell, and M. A. Green, "Effective light trapping in polycrystalline silicon thin-film solar cells by means of rear localized surface plasmons," Appl. Phys. Lett. **96**, 261109 (2010).
18. C. V. Thompson, "Solid-state dewetting of thin films," Annu. Rev. Mater. Res. **42**, 399–434 (2012).
19. M. J. Mendes, E. Hernandez, E. Lopez, P. Garcia-Linares, I. Ramiro, I. Artacho, E. Antolin, I. Tobias, A. Marti, and A. Luque, "Self-organized colloidal quantum dots and metal nanoparticles for plasmon-enhanced intermediate-band solar cells," Nanotechnology **24**, 345402 (2013).
20. V. Jovanov, U. Planchoke, P. Magnus, H. Stiebig, and D. Knipp, "Influence of back contact morphology on light trapping and plasmonic effects in microcrystalline silicon single junction and micromorph tandem solar cells," Sol. Energy Mater. Sol. Cells **110**, 49–57 (2013).
21. A. Ingenito, O. Isabella, and M. Zeman, "Opto-electronic evaluation of thin double-textured crystalline silicon wafers," in *39th IEEE Photovoltaic Specialist Conference* (2013).
22. R. Santbergen, T. L. Temple, R. Liang, A. H. M. Smets, R. A. C. M. M. van Swaaij, and M. Zeman, "Application of plasmonic silver island films in thin-film silicon solar cells," J. Opt. **14**, 024010 (2012).
23. R. Brendel, *Thin-Film Crystalline Silicon Solar Cells: Physics and Technology* (Wiley-VCH, 2003).
24. F. J. Beck, S. Mokkapati, and K. R. Catchpole, "Light trapping with plasmonic particles: beyond the dipole model," Opt. Express **19**, 25230–25241 (2011).
25. S. Mokkapati and K. R. Catchpole, "Nanophotonic light trapping in solar cells," J. Appl. Phys. **112**, 101101 (2012).
26. J. Gee, "The effect of parasitic absorption losses on light trapping in thin silicon solar cells," in *20th IEEE Photovoltaic Specialists Conference (PVSC)*, Las Vegas, Sept. 1988, Vol. **1**, pp. 549–554.
27. G. Sun and J. B. Khurgin, *Plasmonics and Plasmonic Metamaterials*, G. Shvets and I. Tsukerman, eds. (World Scientific, 2012).
28. B. G. de Grooth, "Why is the propagation velocity of a photon in a transparent medium reduced?" Am. J. Phys. **65**, 1156–1164 (1997).
29. M. Boccard, C. Battaglia, F.-J. Haug, M. Despeisse, and C. Ballif, "Light trapping in solar cells: analytical modeling," Appl. Phys. Lett. **101**, 151105 (2012).
30. E. Yablonovitch and G. D. Cody, "Intensity enhancement in textured optical sheets for solar cells," IEEE Trans. Electron Devices **29**, 300–305 (1982).
31. H. Tan, L. Sivec, B. Yan, R. Santbergen, M. Zeman, and A. H. M. Smets, "Improved light trapping in microcrystalline silicon solar

cells by plasmonic back reflector with broad angular scattering and low parasitic absorption," Appl. Phys. Lett. **102**, 153902 (2013).

32. NREL, "AM1.5G solar spectrum irradiance data," http://rredc.nrel .gov/solar/spectra/am1.5.

33. C. Pahud, O. Isabella, A. Naqavi, F.-J. Haug, M. Zeman, H. P. Herzig, and C. Ballif, "Plasmonic silicon solar cells: impact of material quality and geometry," Opt. Express **21**, A786–A797 (2013).

34. H. Tan, R. Santbergen, A. H. M. Smets, and M. Zeman, "Plasmonic light trapping in thin-film silicon solar cells with improved self-assembled silver nanoparticles," Nano Lett. **12**, 4070–4076 (2012).

35. U. W. Paetzold, E. Moulin, D. Michaelis, W. Boettler, C. Waechter, V. Hagemann, M. Meier, R. Carius, and U. Rau, "Plasmonic reflection grating back contacts for microcrystalline silicon solar cells," Appl. Phys. Lett. **99**, 181105 (2011).

36. S. K. Ghosh and T. Pal, "Interparticle coupling effect on the surface plasmon resonance of gold nanoparticles: from theory to applications," Chem. Rev. **107**, 4797–4862 (2007).

37. B. Liu and E. J. Heller, "Multiple scattering and plasmon resonance in the intermediate regime," arXiv:1403.4310v1 [cond-mat. mes-hall] (2014).